Development of an Intelligent Real-time Multi-Person Respiratory Illnesses Sensing System using SDR Technology

Mubashir Rehman, Najah Abed Abu Ali*, Sr., Member, IEEE, Raza Ali Shah, Muhammad Bilal Khan, Syed Aziz Shah, Akram Alomainy, Sr., Member, IEEE, Xiaodong Yang, Sr., Member, IEEE, Muhammad Ali Imran, Sr., Member, IEEE, and Qammer H. Abbasi, Sr., Member, IEEE

***Abstract*—Respiration monitoring plays a vital role in human health monitoring, as it is an essential indicator of vital signs. Respiration monitoring can help determine the physiological state of the human body and provide insight into certain illnesses. Recently, non-contact respiratory illness sensing methods have drawn much attention due to user acceptance and great potential for real-world deployment. Such methods can reduce stress on healthcare facilities by providing modern digital health technologies. This digital revolution in the healthcare sector will provide inexpensive and unobstructed solutions. Non-contact respiratory illness sensing is effective as it does not require users to carry devices and avoids privacy concerns. The primary objective of this research work is to develop a system for continuous real-time sensing of respiratory illnesses. In this research work, the non-contact software-defined radio (SDR) based RF technique is exploited for respiratory illness sensing. The developed system measures respiratory activity imprints on channel state information (CSI). For this purpose, an orthogonal frequency division multiplexing (OFDM) transceiver is designed, and the developed system is tested for single-person and multi-person cases. Nine respiratory illnesses are detected and classified using machine learning algorithms (ML) with maximum accuracy of 99.7% for a single-person case. Three respiratory illnesses are detected and classified with a maximum accuracy of 93.5% and 88.4% for two- and three-person cases, respectively. The research provides an intelligent, accurate, continuous, and real-time solution for respiratory illness sensing. Furthermore, the developed system can also be deployed in office and home environments.**

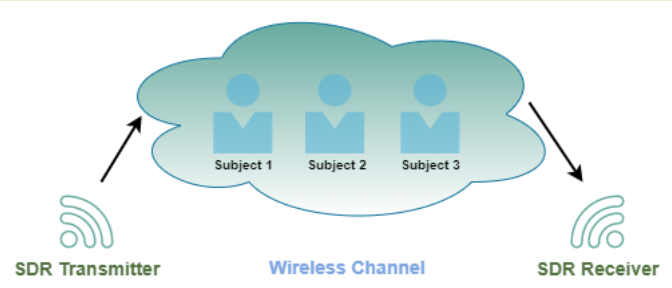

***Index Terms*—Respiratory illness, non-contact, RF sensing, USRP, SDR**

I. Introduction

Respiration is a crucial physiological process in all living organisms. In humans, during this process, air containing oxygen is inhaled into the lungs, where the exchange of gases occurs across the alveolar membrane [1]. As part of this process, carbon dioxide is excreted into the air through the mouth and nose. The process, including the inspiration to expiration, is called a respiration cycle. Respiration is considered one of the vital signs of humans and can be used to detect the progression of severe health issues. Sensing respiratory illnesses can help predict extreme medical events, including cardiac arrest or admission to the intensive care unit [2-3]. Numerous recent studies proved that respiratory illness is more significant than other vital signs such as pulse and blood pressure in distinguishing between healthy and sick persons [4]. Humans take respiratory health for granted and often ignore that the lungs are their vital organs and are susceptible to injury and infections. According to a study by the World Health Organization (WHO), respiratory illnesses are one of the leading causes of disability and death worldwide [5]. Respiratory illnesses contain chronic respiratory diseases, including asthma, chronic obstructive pulmonary disease, and lung cancer [6]. Various factors can trigger respiratory

"This work was supported by Zayed Health Center at UAE University under Fund code G00003476."

Mubashir Rehman and *Najah AbuAli are with the Faculty of Information Technology in the United Arab Emirates University (UAEU), Abu Dhabi, UAE (Correspondence e-mail: najah@uaeu.ac.ae). Mubashir Rehman is also with Department of Electrical Engineering, HITEC University, Taxila, Pakistan. Raza Ali Shah is with Department of Electrical Engineering, HITEC University, Taxila, Pakistan. Muhammad Bilal Khan is with Department of Electrical and Computer Engineering, COMSATS University Islamabad, Attock, Pakistan. Syed Aziz Shah is with the Centre for Intelligent Healthcare, Coventry University, Coventry U.K. Akram Alomainy is with the School of Electronic Engineering and Computer Science, Queen Mary University of London, London, UK. Xiaodong Yang is with the School of Electronic Engineering, Xidian University, Xi'an, China. Qammer. H. Abbasi and Muhammad Ali Imran are with the James Watt School of Engineering, University of Glasgow, Glasgow, U.K. Muhammad Ali Imran is also with Artificial Intelligence Research Centre (AIRC), Ajman University, UAE.

illnesses, such as smoking, heavy air pollution, malnutrition, and job-related disorders [7]. Still, the most common factor is exposure to viruses, including the influenza virus or COVID-19. Accurately identifying respiratory illnesses is vital for treatment as respiratory illnesses' symptoms are quite similar, resulting in misdiagnosis. This may lead to devastating consequences by further spreading the diseases and infections. Hence, an accurate diagnostic discriminator is essential for timely prognosis and suitable actions [8-10].

There is a variety of respiratory illnesses discussed in the literature. Here in this research work, nine respiratory illnesses are considered. The description of each respiratory illness is presented as follows. The respiration with a regular pattern and rate is called eupnea, and it has 12-24 respiratory cycles per minute for an adult at rest. But due to various medical conditions, respiration can lose its regular rhythm, resulting in several respiratory illnesses. These illnesses can alter the respiratory pattern and rate, which can be shallow, deep, or fast. Other respiratory illnesses include bradypnea, tachypnea, biot, kussmaul, sighing, cheyne stokes, central sleep apnea (CSA), and cough. Bradypnea is a kind of illness that

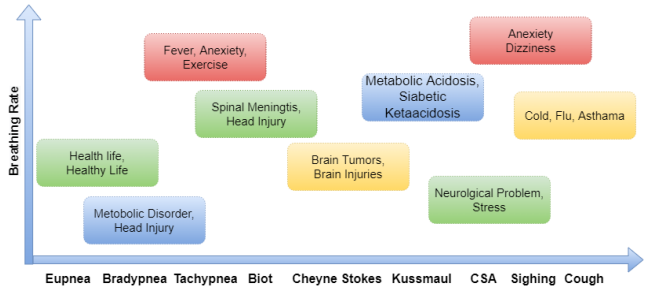

Fig. 1. Respiratory Illnesses and Causes

results in slow and shallow respiration having a uniform pattern and rhythm, with the respiratory cycle less than 12 per minute. In tachypnea, the respiratory rate becomes faster than eupnea, and it is usually more than 24 respiratory cycles per minute. Biot respiration is distinguished by deep breaths followed by frequent apnea episodes, and kussmaul is fast and deep respiration. In sighing, respiration is normal with interspersed sighs. Cheyne stokes respiration has a steady rise and drop in respiration rate, whereas in CSA, respiration stops during sleep. A cough is the contraction of respiratory muscles, which compress the air in the lungs. This contraction is followed by the glottis closure after inhalation of air [11]. It occurs instantly before the sudden reopening of the glottis, which causes rapid air exhalation from the lungs to clear out respiratory passages. Cough is a significant indication of respiratory illnesses [12] and a natural defense system of the human body to protect the respiratory system [13]. The causes of all respiratory illnesses against respiration rate are provided in figure 1. It is evident from figure 1 that various respiratory illnesses have different breathing rates, e.g., tachypnea has high breathing rate than bradypnea.

Evaluating abnormalities in respiratory activities has been considered a primary medical diagnosis tool for respiratory illnesses for centuries but has relied on the availability of appropriately trained personnel. Consequently, timely disease diagnoses are not made due to a lack of such personnel during times of need. As a result, the demand for medical facilities that monitor respiratory illnesses in real time without the physical presence of medical professionals has increased significantly. Modern sensors and advanced signal processing techniques now make this a clear possibility. These latest techniques can detect respiratory illnesses without visiting medical facilities, reducing the hospital's load. Furthermore, these methods provide a self-monitoring system for respiratory illness sensing at home and offices, which can be essential during the previously prevailing COVID pandemic. A non-contact system is developed for sensing various respiratory illnesses in this research work. The developed system can carefully examine the patients in real-time and classify respiratory illnesses using ML algorithms. Utilizing SDR devices and omnidirectional antennas, the proposed system measures the imprints of respiratory activities on CSI, providing portable, scalable, flexible, and multifunctional solutions for respiratory illness sensing.

II. Related Work

The technologies for respiratory illness sensing, as shown in figure 2, are categorized into two types depending on the methods of usage and operation. These technologies are either contact-based or non-contact-based. In contact-based technologies, there is direct contact with the human body. But, in non-contact technologies, respiratory illness sensing is done without contact with the human body. Non-contact sensing has clear advantages compared to contact-based sensing, as it provides long-term real-time monitoring without affecting the patient's comfort and privacy concerns.

2.1 Contact-Based Respiratory Illness Sensing

Several technologies are discussed in the literature based on contact-based sensing, as given in table I and described below.

2.1.1 Air Temperature Measurement

During respiration, the exhaled air from the human body is usually warmer than the inhaled. This exhaled air temperature can be used for sensing respiratory illness. Various types of sensors are used in the literature for this purpose. These sensors are electric-based (i.e., pyroelectric, thermocouples, and thermistors) or fiber optic. The description of these sensors is provided as follows. The pyroelectric effect is mainly a change in surface charge in response to the change in temperature. The literature uses the pyroelectric effect to detect the changes in exhaled air temperature [14]. Furthermore, a thermocouple produces a temperature-dependent voltage due to the thermoelectric effect, which is basically the existence of an electric potential once two metals are attached in the loop by keeping two junctions at different temperatures. Thermocouples are exploited in the literature to measure the exhaled air temperature for respiratory illness sensing [15]. The thermistor is a kind of resistor whose resistance changes with a change in the temperature [16]. Thermistor sensors are used in the literature for sensing exhaled air temperature. Fiber optic sensors are also used to find the exhaled air temperature during

expiration [17]. All these sensors need to expose to exhaled air, which makes their measurement intrinsically intrusive; however, these sensors provide respiration measurement overtime on a breath-by-breath basis.

2.1.2 Airflow Measurement

Different airflow sensors can measure air volume and flow being exhaled and inhaled during respiration. The temporal trend of airflow volume can measure the respiratory rate and illnesses. These sensors include hot-wire anemometers, turbine flowmeters, differential flowmeters, and fiber-optic-based flowmeters. Hotwire anemometers contain heated wires swapping heat with the flow of fluid [18]. This heat exchange facilitates measuring respiratory rates and illnesses. In contrast, turbine flowmeters have a turbine with flat blades for externally carrying the ventilated air towards the distributor. While the distributor is mainly a cylinder having slits on the surface. The number of turbine revolutions is usually measured with the help of a phototransistor that measures the blade passage in front of it, delivering the respiratory rate. This mechanism helps in respiratory illness sensing [19]. Differential flowmeters consist of pipes with a pneumatic resistance through the gas flows. This resistance aids in measuring the respiratory rate by transducing the gas flow rate within a pressure drop [20]. In fiber-optic-based sensors, the variations of light power coupled are measured with the bending of fiber produced due to exhaled or inhaled airflow. Hence, the light power calculated with the help of a photodetector denotes the sensor output, which provides the respiratory flow rate [21]. These airflow sensors need to contact the inhaled and exhaled air, which makes their respiratory illness sensing intrusive; however, their small size helps in unobstructed measurements.

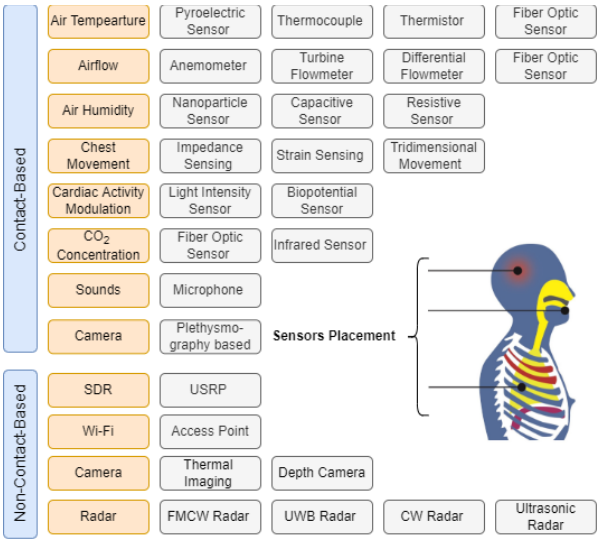

Fig. 2. Related Work

2.1.3 Breathing Air Humidity Measurement

The exhaled and inhaled air have different water vapor content. Hence, the difference in contents of water vapor between inhaled and exhaled air can be used for respiratory illness. Various proposed sensors in the literature include nanoparticle, capacitive, and resistive sensors. Respiratory illness sensing using nanoparticle sensors is based on the principle that the resistance of a thin film of SiO_2 nanoparticles changes non-linearly with respiratory rate variation, which can be used for respiratory illness sensing [22]. The capacitive sensors for respiratory illness sensing work on the principle that with variations of the dielectric characteristics of the material introduced between the two electrodes, the capacitance varies [23]. At the same time, resistive sensors work on the principle that electrical impedance varies with humidity. Therefore, respiratory illness sensing is done by measuring the changes in the sensing films' conductivity [24]. All these humidity sensors measure the variations in water vapor content within exhaled and inhaled air, which demand continuous intrusiveness.

2.1.4 Chest Movement Sensing

The process of respiration is performed with the help of the diaphragm, respiratory muscles, and intercostal muscles. This causes chest movement during respiration which can help sense the respiratory illness. Various approaches and sensors are explored in the literature for this chest movement sensing. The changes in transthoracic impedance are used to measure respiratory illness [25]. Likewise, the chest well strain generated due to respiration is exploited for respiratory illness sensing [26]. The record of tridimensional movements of the thorax (e.g., thorax inclination, acceleration, and velocities by using accelerometers, gyroscopes, and magnetometers) is used for respiratory activity sensing [27]. These chest movement sensing-based sensors are very appropriate for respiratory illness sensing as these sensors are embedded in clothes easily during their manufacturing. This makes these sensors relatively unobtrusive, but wires are necessary for the power supply.

2.1.5 Cardiac Activity Modulation

Respiratory illness sensing can be performed by measuring cardiac activity, as respiration modulates cardiac activity. Light intensity sensors or biopotential sensors are exploited in the literature for this purpose. Photoplethysmography (PPG) is an optical method that can calculate the variations in the blood volume in the tissue over time. Usually, these variations are measured by fingers or toes using pulse oximeters [28]. In electrocardiography (ECG), biopotential sensors measure the electrical activity generated due to the potential difference in heart muscle for every heartbeat. ECG signals are usually measured by calculating the potential difference between two locations on the surface of the human body. Respiratory illness sensing using ECG is demonstrated by [29]. These light intensities and biopotential sensors are used for respiratory illness as they provide low invasiveness, low cost, low energy consumption, and easy integration in wearable systems. However, their sensitivity is highly affected due to movements other than respiration.

2.1.6 Carbon dioxide Concentration

As respiration is a cellular process, oxygen and carbon dioxide content differs between the exhaled and inhaled air. Various chemical sensors are used to estimate respiratory illness from the carbon dioxide concentration difference between exhaled and inhaled air. These sensors include infrared sensors and fiber optic sensors. Fiber optic sensors are used for gas concentration measurement by investigating variation at the fiber's distal end where a carbon dioxide-sensitive material is placed. [30]. Infrared sensors are exploited as spectroscopic sensors due to their characteristic absorption for measuring

carbon dioxide concentration. But to deliver the exhaled and inhaled gas to the sensor [31]. All these carbon dioxide concentration measurement sensors need to expose to exhaled air which makes them quite intrusive. Furthermore, the accuracy of these sensors is affected due to their cross-sensitivity to other gas components.

2.1.7 Breathing Sounds Measurement

The sound produced due to throat and airways during respiration may be exploited for respiration illness sensing [32]. The working principle behind these sound sensors is based on their sensitivity to physical changes in the environment surrounding the sound source. The microphones are commonly sensors for measuring variation in air pressure generated by the sound waves. Microphone sensors are effective in respiratory illness sensing as they are easily integrated into wearable devices. Though, the measurement of these sensors is vulnerable to background noise.

TABLE I
RELATED STUDY

Illness Sensing	Methods	Devices/Sensors Type	References
Contact-Based	Air Temperature	Pyroelectric	[14]
		Thermocouple	[15]
		Thermistor	[16]
		Fiber Optic Sensor	[17]
	Airflow	Anemometer	[18]
		Turbine Flowmeter	[19]
		Differential Flowmeter	[20]
		Fiber Optic Sensor	[21]
	Air Humidity	Nanoparticle Sensor	[22]
		Capacitive Sensor	[23]
		Resistive Sensor	[24]
	Chest Movement	Impedance Sensing	[25]
		Strain Sensing	[26]
		Tridimensional Movements	[27]
	Cardiac Activity Modulation	Light Intensity Sensor	[28]
		Biopotential Sensor	[29]
	Carbon dioxide Concentration	Fiber Optic Sensor	[30]
		Infrared Sensor	[31]
	Sounds	Microphone	[32]
	Mobile Camera	Plethysmography Based	[33]
Non-Contact Based	Radar	FMCW Radar	[34]
		UWB Radar	[35]
		CW Radar	[36]
		Ultrasonic Radar	[37]
	Wi-Fi	RSS Based	[38]
		CSI Based	[39]
	Camera	Thermal Imaging Camera	[41]
		Depth Camera	[42]
	SDR	USRP Based	[43]

2.1.8 Mobile Camera Based

Plethysmography measures volume changes in different areas of the body. Cell phone cameras can be used for plethysmography by measuring variations in blood volume based on recorded light intensity [33].

2.2 Non-Contact-Based Respiratory Illness Sensing

In non-contact respiratory illness sensing techniques, the devices or sensors do not contact the human body. Therefore, avoiding the privacy and discomfort issues. Though, some of the non-contact techniques require costly and complex devices. In the following section, several non-contact respiratory illness sensing technologies are given in Table I and presented below.

2.2.1 Radar-Based

Various radar-based technologies have also been exploited for respiratory illness sensing. These technologies include frequency modulated continuous wave (FMCW) radar, ultra-wideband (UWB) pulse radar, continuous wave (CW) doppler Radar, and ultrasonic-based radar. FMCW works on the principle that the frequency variations of the emitted radar signals permit the distance measurement to the subject over time. The respiration activity of the subject changes the reflected waveform' amplitude resulting in sensing the respiratory illness [34]. In the case of UWB radar, short-duration pulses are transmitted towards the target and received back after reflection; the time delay between the transmitted pulse and the received echo is utilized to measure the distance between the target and the radar, which in return helps in respiratory illness sensing [35]. For the CW doppler radar case, RF signals are transmitted and modulated by chest and abdomen movements [36]. In an ultrasonic-based radar case, self-injection locked ultrasound radar is exploited to measure respiration activities ad illnesses [37]. All these radar-based techniques provide a suitable non-contact solution for respiratory illness sensing; but this demands complex dedicated equipment, and regular usage of such devices may cause the radiational hazard.

2.2.2 Wi-Fi-based

In the literature, Wi-Fi access points are used for respiratory illness sensing and are categorized into two types, radio signal strength (RSS) and channel state information (CSI) based. RSS is a robust measure of the radio signal received at the receiver. RSS provides a coarse-grained measurement that is easily affected due to the multipath effect. [38] used of RSS measurements between Wi-Fi links to recognize respiratory illnesses and rates. On the other hand, CSI provides more detailed and fine-grained information by measuring the power attenuation due to the multipath. [39] proposed a non-contact system for sensing respiratory illness exploiting CSI acquired from Wi-Fi access points. This Wi-Fi-based sensing provides various benefits such as easy availability of hardware and cost-effectiveness. Still, it also shows a few drawbacks like deprivation of flexibility and scalability [40].

2.2.3. Camera-Based

Several techniques discussed in the literature for respiratory illness sensing include thermal imaging and depth cameras. The temperature around the nose fluctuates during respiration; therefore, infrared thermography can detect respiratory illnesses [41]. Furthermore, respiratory activity can be extracted from examining human respiratory motions captured by a video camera. For this purpose, a depth camera has been used in previous studies [42]. The camera-based technologies provide reasonable solutions. Still, they have some drawbacks, such as susceptibility to ambient heat for the thermal camera case and high computational cost for the case of depth cameras.

2.2.4. SDR Based

Several systems for SDR-based respiratory monitoring have been presented in the literature. [43] suggested a contactless

SDR-based system for predicting breathing and heart rate based on small chest motions. This is accomplished by employing directional antennas and a vector network analyzer (VNA). Furthermore, the performance of the proposed system is evaluated by varying the subject's distance from the antennas. In addition, a scenario involving monitoring through walls is considered. [44] uses SDR to implement a multi-frequency, continuous-wave radar system for monitoring breathing patterns at predetermined distances. The channel frequency response (CFR) is used in [45] to identify minute variations in OFDM subcarriers caused by human motion over wireless channels. As illustrated in Figure 22, the developed platform correctly identified hand waving, irregular coughing, and a variety of respiratory diseases. [46] uses USRP to create a contactless respiratory illness sensing system. This platform used CSI to record the minute movements caused by respiratory activity and identified three distinct breathing patterns. While in [47], a system's design is validated by first analyzing the coefficient of determination (CFR) for multiple simulated channels, this is not the case here. ML algorithms successfully classify a few respiratory diseases. In [48], SDR-based breathing pattern sensing is used to detect and classify six abnormal breathing patterns. This work is expanded upon in [45] by classifying up to eight breathing patterns.

III. System Design

The system design consists of three main blocks: wireless signal sensing, data preprocessing, and machine learning, as shown in figure 3. The description of each block is given below:

3.1 Wireless Signal Sensing

The wireless signal sensing block contains a transmitter, wireless channel, and receiver. Each transmitter and receiver include a host PC and USRP. The host PC runs SDR's software functionality in Laboratory Virtual Instrument Workbench (LabVIEW) software. While USRP model NI-2922 is used to perform RF functionality of SDR. Each USRP kit is loaded with a single omnidirectional antenna. The purpose of the transmitter is to generate an RF signal, which the receiver will receive after passing the wireless channel. The developed system detects various breathing illnesses by observing CSI variations of the wireless channel due to human respiration. The description of the wireless sensing block is proved as follows:

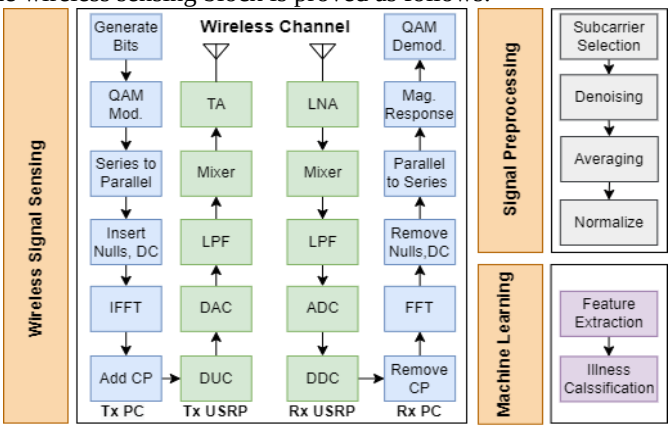

Fig. 3. System Design

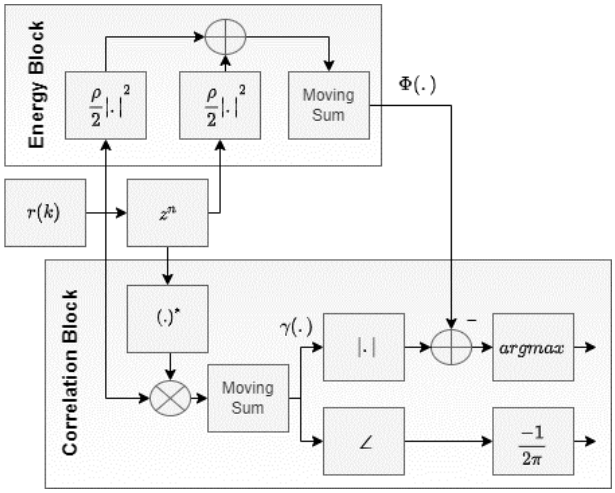

Fig. 4. Van de Beek Algorithm

A. Transmitter

The transmitter is comprised of the host PC and USRP. The host PC on the transmitter side generates pseudo-random bits and changes into quadrature amplitude modulation (QAM) symbols. First, these symbols are separated into parallel streams, and then reference symbols are included. These reference symbols aim to estimate the channel on the receiver side. Afterward, nulls are added at the frame border, and DC is added at the frame center. Now inverse fast Fourier transform (IFFT) is utilized to translate this frequency domain signal into a time-domain signal.

Furthermore, a cyclic prefix (CP) is added to each frame by replicating the last one-fourth samples of the OFDM frame at the start. This CP will aid in removing time and frequency offset on the receiver side. Later, this synthesized data in the transmitter PC is delivered to transmitter USRP over a gigabit ethernet wire. In USRP, different operations like digital up-conversion (DUC), digital to analog conversion (DAC), and low pass filtering (LPF) are performed. Then the resultant signal is mixed up to specified user frequency user a mixer. Eventually, the mixed signal is passed to the transmit amplifier to adjust its gain and broadcast it through an omnidirectional antenna.

B. Wireless Channel

The wireless channel is exploited for information regarding various respiratory illnesses due to tiny variations in CSI. Whenever an individual is found within the experimental area, an additional supplementary channel is created due to its respiratory movements, resulting in CSI variation. Consequently, these CSI variations are exploited for breathing illnesses sensing. The transmitter USRP continuously transmits the signal received at the receiver after traveling through the wireless channel. This received signal has information about several human aspects, such as postures and respiratory illnesses. This information is received at the receiver as CSI's variations.

C. Receiver

The signal is primarily received at the receiver through an omnidirectional antenna. After which, the received signal is moved through low noise amplification (LNA) to reduce the noise factor. Then signal mixing is performed to translate it

back into a baseband signal. Subsequently, the baseband signal passed through different operations like low pass filtering, analog to digital conversion (ADC), and digital down-conversion (DDC). The signal is then moved to the receiver computer over a gigabit ethernet wire. The received signal, r(n) holds the wireless CSI, containing information about channel effects and noise. The time offset (TO) gives rise to the rotation of data symbols. In contrast, the carrier frequency offset (CFO) gives rise to a shift of all the subcarriers, which spoils the orthogonality of the subcarriers and generates inter-channel interference. Consequently, estimation of these offsets is required at the receiver. TO is modeled as a delay in the channel impulse response, while CFO is modeled as a multiplication of each s(n) sample by $e^{\frac{j2\pi\varepsilon n}{N}}$. Where ε is the normalized CFO and N is the number of subcarriers. While the received samples can now be modeled as shown in (1):

$$r(n) = c(n) * s(n-\theta)e^{\frac{j2\pi\varepsilon n}{N}} + N(n) \quad (1)$$

where $c(n)$ is the channel response, θ is the unknown TO, ε is an unknown CFO and $N(n)$ is the additive noise. This paper uses the van de Beek algorithm to estimate CFO and TO [48]. This algorithm is also exploited for frame synchronization in order to eliminate the CP correctly. Figure 4 illustrates the mechanism of the algorithm. The algorithm measures the estimate of $\grave{t}_{OS}$ and $\grave{f}_{OS}$ by applying (2) and (3), respectively:

$$\grave{t}_{OS} = \arg\max\{|\gamma(t_{OS}| - \rho\Phi(t_{OS})\} \quad (2)$$

$$\grave{f}_{OS} = -\frac{1}{2\pi}\angle\gamma(\grave{t}_{OS}) \quad (3)$$

where $\gamma(t_{OS})$ provided in (2) is used to estimate time offset $\grave{t}_{OS}$ and frequency offset $\grave{f}_{OS}$. The magnitude of $\gamma(t_{OS})$ is compensated by energy term $\Phi(t_{OS})$ and peaks at time instant, which provides $\grave{t}_{OS}$, while its phase at this time instant is proportional to $\grave{f}_{OS}$. The $\gamma(t_{OS})$ is the correlation between two pairs of L samples of OFDM frame that are N samples apart. $\Phi(t_{OS})$ is the energy part and ρ is the magnitude of the correlation coefficient provided in (4,5,6), respectively.

$$\gamma(m) = \sum_{n=m}^{m+L-1} r(n)r^*(n+N) \quad (4)$$

$$\Phi(m) = \frac{1}{2}\sum_{n=m}^{m+L-1} |r(n)|^2 + |r(n+N)|^2 \quad (5)$$

$$\rho = \frac{|E\{r(k)r^*(k+N)\}|}{\sqrt{E\{|r(k)|\}^2\, E\{|r(k+N)|\}^2}} \quad (6)$$

After removing TO and CFO using the van de Beek algorithm, FFT is applied to convert this time-domain signal into a frequency domain signal. Later, nulls, DC, and reference signals are removed, and the magnitude response is calculated for the frequency domain signal. Eventually, QAM demodulation is applied to convert symbols back into the bitstream.

3.2 Signal Preprocessing

After the raw data collection through a wireless signal sensing bock, the respiratory data is passed through a signal preprocessing block to retrieve valuable information and eliminate noise. The OFDM signal extracted at the receiver is in the frequency domain and contains both magnitude and phase information. Although in this research work, only magnitude information is exploited for sensing respiratory illnesses. The signal preprocessing has multiple steps, and each is described as follows:

A. Subcarriers Selection

Amplitude information for a group of subcarriers is acquired for all respiratory illness activities. It is noted that each subcarrier's amplitude is distinct for respiratory activity. Few subcarriers are more sensitive to the respiratory activity and have high amplitude variations. Variance is calculated to check the sensitivity of the subcarrier to respiratory activity. The threshold value selected for variance was 0.0001. All subcarriers with minor variance values less than the threshold are discarded. For variance calculation, the following (7) is applied to respiratory signals, which can be given as:

$$var_k = \frac{1}{n-1}\sum_{i=0}^{n-1} x_i - \bar{x}_k \quad (7)$$

Here var_k and $\bar{x}_k$ is the variance and mean of k_{th} subcarrier. While x_i is the i_{th} sample value of k_{th} subcarrier and n represent the total number of sample values.

B. Denoising

After the subcarrier selection, the next step is denoising, which removes outliers. For this purpose, wavelet filtering is applied, eliminating the outliers and preserving the data's sharp transition. Hence, avoiding the loss of valuable information during the denoising step. The soft heuristic threshold is applied with scaled noise parameters for wavelet filtering in this research work.

C. Averaging

To further refine data and remove high-frequency noise components, averaging is performed. For this purpose, a moving average filter having a window length of 8 is applied. Finally, (8) is used for averaging the respiratory signal as follows:

$$x_{avg}[n] = \frac{1}{L}\sum_{i=0}^{L-1} x[n-i] \quad (8)$$

Here $x_{avg}[n], x[n]$ represent the current output and current input, respectively, and L represents the length of the window of the moving average filter.

D. Normalizing

The final step in signal preprocessing is normalizing. This step aims to keep respiratory signal data within a fixed range of 1 and -1. This helps in scaling respiratory illness signals by keeping them within the same range. The signal normalizing is performed by the following (9):

$$x_{norm}[n] = \frac{x_{avg}[n] - offset}{scale} \quad (9)$$

Here $x_{norm}[n]$ represents the normalized data and $x_{avg}[n]$ represents the input data. The normalized respiratory signal is obtained by adjusting some scaling and offset values.

3.3 Machine Learning

The machine learning block contains two subblocks which are discussed below:

TABLE II
STATISTICAL FEATURES

Sr. #	Features	Expression	Description
1.	Mean	$\bar{x} = \frac{\sum_{i=1}^{n} x_i}{n}$	Data mean
2.	Standard deviation	$x_{SD} = \sqrt{\frac{1}{n}\sum_{i=1}^{n}(x_i - \bar{x})^2}$	Data dispersion relative to mean
3.	Peak-to-peak value	$x_{p-p} = x_{max} - x_{min}$	Maximum to minimum value difference
4.	RMS	$x_{RMS} = \sqrt[2]{\frac{1}{n}\sum_{i=1}^{n} x_i^2}$	Square root of mean square data
5.	Kurtosis	$x_{Kur} = \frac{\frac{1}{n}\sum_{i=1}^{n}(\lvert x_i\rvert - \bar{x})^4}{x_{SD}{}^4}$	Measure peaks of frequency distribution
6.	Skewness	$x_{Skew} = \frac{\frac{1}{n}\sum_{i=1}^{n}(\lvert x_i\rvert - \bar{x})^3}{x_{SD}{}^3}$	Measure of symmetry in data distribution
7.	Shape Factor	$x_{SF} = \frac{x_{RMS}}{\frac{1}{n}\sum_{i=1}^{n}\lvert x_i\rvert}$	Square root of variance
8.	Crest Factor	$x_{CF} = \frac{max_i\lvert x_i\rvert}{x_{RMS}}$	Peak height value to RMS value
9.	Impulse Factor	$x_{IF} = \frac{max_i\lvert x_i\rvert}{\bar{x}}$	Peak height value to mean value
10.	Entropy	$x_{Ent} = \sum_{i=-n}^{n} hist(x_i)\, ln_2(hist(x_i))$	Measure of randomness of data
11.	Maximum Frequency value	$X_{fmax} = Max(FFT(x))$	Maximum of frequency components

A. Feature Extraction

Feature extraction means reducing the number of features required to describe a data set. However, if the number of features is large, then the number of observations stored in a dataset causes the problem of overfitting during the training of the ML model. Therefore, feature extraction is vital, and developing an ML model with high dimensionality (large features) is time-consuming and expensive. Hence, extracting only useful features can enhance the performance of the ML model [49]. Various time and frequency domain features are extracted in this research work, and a description is provided in Table II.

B. Respiratory Illnesses Classification

ML algorithms are used for respiratory illnesses by developing a classification model. These algorithms can classify nine breathing illnesses, and their performance relies on the type and size of the dataset. Therefore, various algorithms provide different performances depending on the dataset, while the performance of each algorithm can be enhanced by enhancing the dataset size.

The performance evaluation is typically based on the accuracy, training time, and prediction speed. A confusion matrix is exploited for this purpose. The rows in the confusion matrix represent the true classes. Likewise, the predicted classes are represented by the columns. On the other hand, the diagonal entries in the confusion matrix correspond to instances where the actual class and predicted class are matched. All entries other than the diagonal represent instances where the ML algorithm has shown poor performance. In this study, the cross-validation (CV) technique is used to evaluate the model, while the algorithm performance is evaluated on new data by providing predictions that were not previously trained. The whole dataset is first split into smaller subsets for training the algorithm in this CV method. Then, CV selects the random subsets into the training and testing groups. Later, supervised learning techniques are used to train and test datasets to evaluate the performance. This procedure is repeated several times, and the average error is computed. CV helps in avoiding overfitting and underfitting. Here in this research work, 5-fold cross-validation is used.

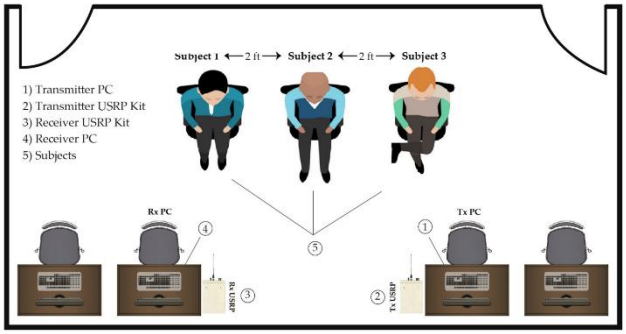

Fig. 5. Experimental Setup

IV. EXPERIMENTAL SETUP

The experimental setup for data collection of breathing illnesses consists of two host computers and USRPs, as shown in figure 5. Each USRP is loaded with one omnidirectional antenna for transmission and reception purposes. The omnidirectional antenna helps capture respiratory illness information in the line of sight (LOS) and non-LOS scenarios. The USRP devices are positioned parallel to the subject's abdomen. The description of each respiratory illness is provided to all subjects. Each subject is requested to sit in a calm posture and perform each breathing illness activity professionally as per medical data. A total of ten subjects are invited to perform respiratory activities, and the characteristics of all subjects are provided in Table III. The developed experimental setup is utilized to collect single-person and multi-person case data. Each subject is asked to perform nine respiratory illnesses for single-person cases, including eupnea. While for multi-person cases, two-person and three-person cases are considered. Both subjects are asked to perform three respiratory illnesses for two-person cases, including eupnea, bradypnea, and tachypnea, which results in six scenarios. All three subjects are asked to perform three respiration illnesses for a three-person case, including eupnea, bradypnea, and tachypnea, resulting in nine scenarios. Ten datasets are collected for all respiratory illnesses for each multi-person case, and each activity is performed for 28 seconds.

TABLE III
SUBJECTS CHARACTERISTICS

Variables	Mean	Min-Max
Age (Years)	30.8	24-37
Height (In)	67.4	61-70
Weight (Kg)	72.5	51-91
Body Mass Index	25.2	16.1-37.9

V. Results and Discussions

This section is divided into two subsections. The first subsection presents and discusses the results of respiratory illnesses in single and multi-person cases. While in the second subsection, classification results of ML algorithms for single and multi-person cases are presented and discussed.

5.1 Respiratory Illness Sensing

This section describes respiratory illness sensing exploiting SDR-based sensing in detail. All respiratory illness activities are imitated ten times, and before performing each activity, subjects are familiarized with the characteristics of all respiratory illnesses via proper training and guidance. The CSI's amplitude response is used to detect and analyze all respiratory illnesses. The variation in amplitude response is obtained for respiratory illness activity over 3500 samples.

A. Single-person case

For single person case, nine breathing illnesses are considered, and graphs from subject 2 are presented in figure 6 and discussed as follows:

Eupnea is normal respiration with the usual pattern and rate. Adults usually have 12-24 respiratory cycles per minute at rest in eupnea. The subject is asked to do respiration normally to perform this respiration activity. Figure 6(a) shows 12 respiration cycles in a half-minute, which verifies that this is eupnea respiration. Bradypnea is a shallow and slow respiration illness. Each subject is asked to do respiration slower than the normal rate to mimic the respiration illness. Figure 6(b) shows 6 respiration cycles in a half-minute, which verifies that this is bradypnea respiration. Tachypnea is a fast and shallow respiratory illness. To perform this respiratory illness, each subject is asked to do respiration faster than the normal rate. Figure 6(c) shows 15 respiration cycles in a half-minute, which verifies that this is tachypnea respiration as biot is deep respiration with gradual periods of apnea. Figure 6(d) shows that it is biot respiration, as deep and fast respiration followed by apnea is observed. Cheyne stokes is characterized by a gradual increase and decrease in respiration rate, and by observing figure 6(e), it can be seen that it is cheyne stokes respiration. As Kussmaul is fast and deep respiration, figure 6(f) verifies Kussmaul respiration. Figure 6(g) shows that it is a CSA respiration as regular respiration cycles are observed, followed by apnea. Furthermore, sighing is respiration punctuated with frequent deep, and figure 6(h) verifies that it is sighing respiration. As cough is the respiratory muscle contraction, three coughs can be observed during normal respiration from figure 6(i).

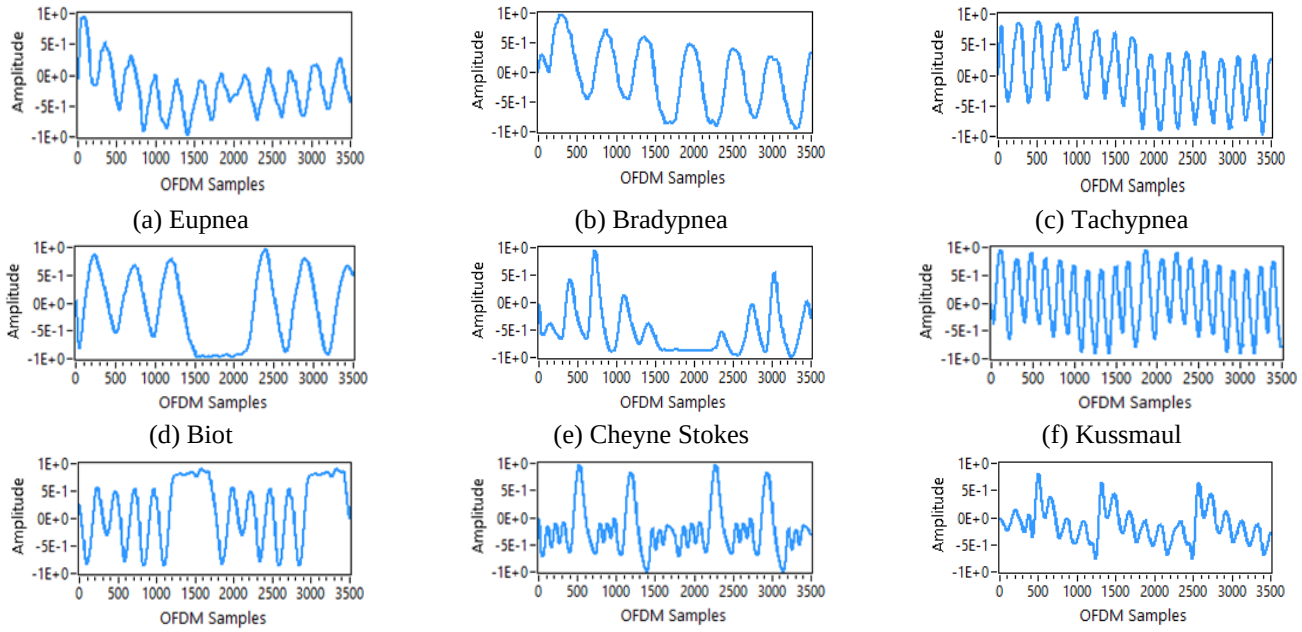

(a) Eupnea (b) Bradypnea (c) Tachypnea

(d) Biot (e) Cheyne Stokes (f) Kussmaul

(g) Central Sleep Apnea (h) Sighing (i) Cough

Fig. 6. Respiratory Illness's Graphs for Single Person Case

(a) Two-Persons Case (b) Three-Persons Case

Fig. 7. Respiratory Illness's Graphs for Multi-Persons Case

B. Two-person and three-person case

Both subjects are asked to perform three respiratory illnesses for a two-person case, including eupnea, bradypnea, and tachypnea. This results in six scenarios where all subjects mimic the same or different respiratory illnesses. Here for illustration purposes, the result for only one scenario is

presented in figure 7(a), in which one subject is performing eupnea respiration while the other is performing bradypnea respiration. Likewise, for a three-person case, all three subjects are asked to perform three respiratory illnesses, including eupnea, bradypnea, and tachypnea. This results in nine different scenarios where all subjects mimic the same or different respiratory illnesses. Here for illustration purposes, the result for only one scenario is presented in figure 7(b), in which all three subjects are doing eupnea respiration. For two and three-person cases, it is impossible to distinguish respiratory illnesses as CSI is obtained due to independent chest movements of all subjects, which makes it impossible to extract each subject's respiratory illness independently.

TABLE IV
CLASS LABEL DETAILS FOR SINGLE-PERSON CASE

Class #	Class Label	Details
1	Eupnea	Normal respiration
2	Bradypnea	Slow and shallow respiration
3	Tachypnea	Fast and shallow respiration
4	Biot	Deep respiration with regular phases of apnea
5	Sighing	respiration punctuated by repeated deep sighs
6	Kussmaul	Deep and Fast respiration
7	Cheyne Stokes	Varying periods of respiration
8	CSA	Respiration followed by apnea
9	Cough	Contraction of respiration muscles

TABLE V
CONFUSION MATRIX FOR SINGLE-PERSON CASE

		Predicted Class									
Fine gaussian SVM	**Class**	1	2	3	4	5	6	7	8	9	**True Class**
	1	98.9	0.2	0.7	0	0	0	0	0.1	0	
	2	0.5	99.3	0.1	0	0	0	0	0	0	
	3	1.0	0.1	98.8	0.1	0	0	0	0	0	
	4	0.1	0	0.1	99.9	0	0	0	0	0	
	5	0	0	0	0	100	0	0	0	0	
	6	0	0.1	0	0	0	99.9	0	0	0	
	7	0	0	0	0	0	0	100	0	0	
	8	0.3	0.1	0.1	0	0	0	0	99.6	0	
	9	0	0	0	0	0	0	0	0	100	
		Predicted Class									
Fine KNN	**Class**	1	2	3	4	5	6	7	8	9	**True Class**
	1	99.0	0.4	0.5	0	0	0	0	0.2	0	
	2	0.3	99.6	0.1	0	0	0	0	0	0	
	3	1.0	0.2	98.7	0	0	0	0	0	0	
	4	0.1	0	0	99.9	0	0.1	0	0	0	
	5	0	0	0	0	100	0	0	0	0	
	6	0	0.1	0	0	0	99.9	0	0	0	
	7	0	0	0	0	0	0	100	0	0	
	8	0.4	0.1	0.1	0	0	0	0	99.5	0	
	9	0	0	0	0	0	0	0	0	100	
		Predicted Class									
Ensemble Bagged Tree	**Class**	1	2	3	4	5	6	7	8	9	**True Class**
	1	99.2	0.4	0.2	0	0	0	0	0.2	0	
	2	0.3	99.5	0.1	0	0	0.1	0	0	0	
	3	0.6	0.1	99.3	0	0	0	0	0	0	
	4	0	0	0.1	99.8	0	0	0.1	0	0	
	5	0	0	0	0	100	0	0	0	0	
	6	0	0	0	0	0	99.9	0	0	0	
	7	0.1	0	0	0	0	0	99.9	0	0	
	8	0.3	0.1	0	0	0	0	0	99.6	0	
	9	0	0	0	0	0	0	0	0	100	
		Predicted Class									
Medium Neural Network	**Class**	1	2	3	4	5	6	7	8	9	**True Class**
	1	94.5	2.2	2.8	0	0	0.1	0.1	0.3	0	
	2	2.5	96.5	0.3	0.1	0	0.2	0	0.4	0	
	3	2.4	0.6	96.3	0.1	0	0.2	0	0.3	0	
	4	0.1	0.1	0.1	99.6	0	0.1	0.1	0	0	
	5	0	0	0	0	100	0	0	0	0	
	6	0	0.3	0	0.1	0	99.5	0	0	0	
	7	0.1	0	0	0	0.1	0.1	99.7	0	0	
	8	0.3	0.4	0.4	0	0	0	0	98.9	0	
	9	0	0	0	0	0	0	0	0	100	

5.2 Respiratory Illness Classification

This section applies several ML algorithms to classify respiratory illness for single-person and multi-person cases. For validation, a five-fold cross-fold is used to predict the accuracy of the fitted model. Additionally, cross-validation also avoids overfitting. Here, a confusion matrix plot in this research work depicts how each algorithm has performed in each class. True positive rate (TPR) is used for this purpose. TPR is the proportion of correctly classified class observations in each true class. Furthermore, accuracy, training time, and prediction

speed are measured and used as evaluation parameters for each algorithm's performance. Accuracy is measured in percentages, prediction speed in observations per second, and training time in seconds.

A. Single-person case

Nine respiratory illnesses are classified using various ML algorithms for a single-person case. Class numbers, labels, and detail of each respiratory illness is given in table IV. The confusion matrix representing TPR is shown in Table V. As shown in table V, all nine respiratory illnesses are classified accurately. The performance evaluation for all algorithms is presented in table VI, and it can be observed that out of four algorithms ensemble bagged tree provided maximum accuracy of 99.7%

B. Two-person case

Three respiratory illnesses are considered for the two-person case, which results in six different scenarios. Later, ML algorithms are exploited to classify these six scenarios. Class numbers, labels, and detail of each scenario is given in table VII. The confusion matrix representing TPR is shown in table VIII. As can be seen from table VIII that all six scenarios for the two-persons case are classified accurately. The performance evaluation for all algorithms is presented in table IX, and it can be observed that out of four algorithms, the ensemble bagged tree provided a maximum accuracy of 93.3%.

C. Three-person case

Three respiratory illnesses are considered for a three-person case, resulting in nine different scenarios where all persons are doing the same or different respiration. But here, in this research work, only three scenarios are considered. Various ML algorithms are exploited to classify these three scenarios. Class numbers, labels, and detail of each scenario is given in table X. The confusion matrix representing TPR is shown in Table XI. Table XI shows that all three scenarios for the three-person case are classified accurately. The performance evaluation for all algorithms is presented in table XII, and it can be observed that out of four algorithms ensemble bagged tree provided maximum accuracy of 88.4%.

TABLE VI
PERFORMANCE OF ML ALGORITHMS FOR SINGLE-PERSON CASE

Algorithms	Accuracy (%)	Prediction speed (obs/sec)	Training time (s)
Fine gaussian SVM	99.6	~2500	521.3
Fine KNN	99.6	~1200	726.34
Ensemble Bagged Tree	99.7	~22000	1165.2
Medium Neural Network	98.3	~200000	1949.1

TABLE VII
CLASS LABEL DETAILS FOR TWO-PERSON CASE

Class #	Class Label	Details
1	Eupnea-Eupnea	Both person eupnea respiration
2	Bradypnea- Bradypnea	Both person bradypnea respiration
3	Tachypnea-Tachypnea	Both person tachypnea respiration
4	Eupnea- Bradypnea	One person performs eupnea. The other performs bradypnea respiration
5	Eupnea- Tachypnea	One person performs eupnea. The other performs tachypnea respiration
6	Bradypnea- Tachypnea	One person performs bradypnea. The other performs tachypnea respiration

TABLE VIII
CONFUSION MATRIX FOR TWO-PERSON CASE

		Predicted Class						
Fine gaussian SVM	**Class**	**1**	**2**	**3**	**4**	**5**	**6**	**True Class**
	1	83.2	8.2	2.5	0.8	4.9	0.5	
	2	3.7	93.7	0	0.3	1.6	0.7	
	3	1.2	0.5	95.5	0.3	2.2	0.2	
	4	0.5	0.2	0.7	95.9	2.7	0	
	5	5.9	2.5	2.3	1.8	86.6	1.0	
	6	0.4	0.1	0.1	0.1	1.5	97.8	
		Predicted Class						
Fine KNN	**Class**	1	2	3	4	5	6	**True Class**
	1	84.5	7.2	2.5	0.9	4.5	0.4	
	2	2.9	95.6	0.3	0.2	0.5	0.5	
	3	1.6	0.7	94.0	0.2	3.0	0.5	
	4	0.3	0.7	0.2	94.7	4.0	0.1	
	5	7.3	2.1	2.3	3.3	83.2	1.8	
	6	0.3	0.3	0.1	0.1	2.1	97.1	
		Predicted Class						
Ensemble Bagged Tree	**Class**	1	2	3	4	5	6	**True Class**
	1	87.7	6.6	1.4	0.7	3.3	0.3	
	2	1.2	97.4	0	0.3	0.3	0.8	
	3	1.4	0.6	95.3	0.3	2.2	0.3	
	4	0.9	0.4	0.5	95.7	2.4	0.1	
	5	7.0	2.0	2.0	2.1	86.1	0.8	
	6	0.3	0.2	0.1	0.1	1.5	97.7	
		Predicted Class						
Medium Neural Network	**Class**	**1**	**2**	**3**	**4**	**5**	**6**	**True Class**
	1	79.8	9.2	2.2	0.8	7.5	0.5	
	2	4.3	91.1	0.6	0.5	2.7	0.7	
	3	2.4	0.6	93.3	0.5	2.7	0.4	
	4	1.1	0.8	0.3	95.3	2.3	0.1	
	5	7.9	3.4	2.3	2.1	83.2	1.2	
	6	0.6	0.3	0.3	0.1	0.8	97.9	

TABLE IX
PERFORMANCE OF ML ALGORITHMS FOR TWO-PERSON CASE

Algorithms	Accuracy (%)	Prediction speed (obs/sec)	Training time (s)
Fine gaussian SVM	92.1	~24000	16.76
Fine KNN	91.5	~33000	3.81
Ensemble Bagged Tree	93.3	~28000	6.86
Medium Neural Network	90.1	~280000	49.61

TABLE X
CLASS LABEL DETAILS FOR THREE-PERSON CASE

Class #	Class Label	Details
1	Eupnea-Eupnea-Eupnea	All three persons doing eupnea respiration
2	Eupnea- Bradypnea-Tachypnea	All three persons doing different respiration
3	Tachypnea- Tachypnea-Tachypnea	All three persons doing tachypnea respiration

TABLE XI
CONFUSION MATRIX FOR THREE-PERSON CASE

		Predicted Class			
Coarse gaussian SVM	**Class**	1	2	3	**True class**
	1	100	0	0	
	2	6.3	84.5	9.2	
	3	3.0	25.5	71.5	
		Predicted Class			
Fine KNN	**Class**	1	2	3	**True class**
	1	98.2	1.8	0	
	2	6.3	87.5	6.2	
	3	0.4	26.9	72.7	
		Predicted Class			
Ensemble Bagged Tree	**Class**	1	2	3	**True class**
	1	97.2	1.3	1.5	
	2	9.0	85.5	5.5	
	3	6.2	11.1	82.7	

Medium Neural Network	Predicted Class			True class
Class	1	2	3	
1	98.3	0	1.7	
2	11.0	84.1	5.0	
3	16.5	13.8	69.7	

TABLE XII
PERFORMANCE OF ML ALGORITHMS FOR THREE-PERSON CASE

Algorithms	Accuracy (%)	Prediction speed (obs/sec)	Training time (s)
Coarse gaussian SVM	85.2	~8200	82.4
Fine KNN	86.1	~9900	55.4
Ensemble Bagged Tree	88.4	~5300	71.8
Medium Neural Network	84.0	~63000	120.3

VI. CONCLUSION AND FUTURE WORK

This work develops a non-contact SDR-based system for respiratory illness sensing. The developed system provides an accurate, real-time solution for single-person and multi-person cases. An OFDM-based transceiver is designed in this research work, and the variation in CSI is observed due to respiratory activities. Furthermore, these CSI variations are exploited for respiratory illness sensing. Nine respiratory illnesses are considered for the single person, while three are considered for the multi-person case. The developed system can be deployed for any respiratory disease scenario to detect and classify various respiratory illnesses accurately. However, future work is foreseen to improve, such as collecting data from actual respiratory patients not only mimicking the respiratory illness symptoms as proof of concept. Moreover, evaluating the proposed system for more than three-person cases and more respiratory illnesses.

REFERENCES

[1] J. Tu, K. Inthavong, and G. Ahmadi, Computational fluid and particle dynamics in the human respiratory system. Springer Science & Business Media, 2012.

[2] J. F. Fieselmann, M. S. Hendryx, C. M. Helms, and D. S. Wakefield, "Respiratory rate predicts cardiopulmonary arrest for internal medicine inpatients," Journal of general internal medicine, vol. 8, no. 7, pp. 354–360, 1993.

[3] C. Subbe, R. G. Davies, E. Williams, P. Rutherford, and L. Gemmell, "Effect of introducing the Modified Early Warning score on clinical outcomes, cardio-pulmonary arrests and intensive care utilization in acute medical admissions," Anaesthesia, vol. 58, no. 8, pp. 797–802, 2003.

[4] D. R. Goldhill, A. F. McNarry, G. Mandersloot, and A. McGinley, "A physiologically-based early warning score for ward patients: the association between score and outcome," Anaesthesia, vol. 60, no. 6, pp. 547–553, 2005.

[5] F. of I. R. Societies, The global impact of respiratory disease. European Respiratory Society, 2017.

[6] "Health topics," World Health Organization - Regional Office for the Eastern Mediterranean. http://www.emro.who.int/health-topics.html (accessed Feb. 01, 2022).

[7] K. R. Smith, "Fuel combustion, air pollution exposure, and health: the situation in developing countries," Annual Review of Energy and the Environment, vol. 18, no. 1, pp. 529–566, 1993.

[8] Y. Tang, "W, Schmitz JE, Persing DH, Stratton CW," Laboratory diagnosis of COVID-19: current issues and challenges. J Clin Microbiol, vol. 58, no. 6, pp. e00512–e00520, 2020.

[9] M. Bae, S. Lee, and N. Kim, "Development of a robust and cost-effective 3D respiratory motion monitoring system using the kinect device: Accuracy comparison with the conventional stereovision navigation system," Computer methods and programs in biomedicine, vol. 160, pp. 25–32, 2018.

[10] "Question and answers hub." https://www.who.int/emergencies/diseases/novel-coronavirus-2019/question-and-answers-hub (accessed Dec. 21, 2021).

[11] A. A. Abaza et al., "Classification of voluntary cough sound and airflow patterns for detecting abnormal pulmonary function," Cough, vol. 5, no. 1, pp. 1–12, 2009.

[12] S.-H. Cho et al., "Respiratory disease in the Asia-Pacific region: Cough as a key symptom.," in Allergy & Asthma Proceedings, 2016, vol. 37, no. 2.

[13] J. K. Tomori Z., Cough and Other Respiratory Reflexes | Karger Book. Accessed: Dec. 17, 2021. [Online]. Available: https://www.karger.com/Book/Home/219757

[14] Y. P. Huang, M.-S. Young, and C. C. Tai, "Noninvasive respiratory monitoring system based on the piezoceramic transducer's pyroelectric effect," Review of Scientific Instruments, vol. 79, no. 3, p. 035103, 2008.

[15] A. W. Van Herwaarden and P. M. Sarro, "Thermal sensors based on the seebeck effect," Sensors and Actuators, vol. 10, no. 3, pp. 321–346, Nov. 1986, doi: 10.1016/0250-6874(86)80053-1.

[16] T. G. Beckwith and N. L. Buck, Mechanical measurements. Reading, Mass.: Addison-Wesley Pub. Co., 1969. Accessed: Jan. 21, 2022.

[17] D. A. Krohn, T. MacDougall, and A. Mendez, Fiber optic sensors: fundamentals and applications. Spie Press Bellingham, WA, 2014.

[18] H. H. Bruun, "Hot-wire anemometry: principles and signal analysis." IOP Publishing, 1996.

[19] Y. I. Sokol, R. S. Tomashevsky, and K. V. Kolisnyk, "Turbine spirometers metrological support," in 2016 International Conference on Electronics and Information Technology (EIT), 2016, pp. 1–4.

[20] A. Fleisch, "The Pneumotachograph; an apparatus for registering the velocity of breathing air," Pflugers Arch., vol. 209, no. 1, pp. 713–722, Dec. 1925, doi: 10.1007/BF01730956

[21] P. Saccomandi, E. Schena, and S. Silvestri, "A novel target-type low pressure drop bidirectional optoelectronic air flow sensor for infant artificial ventilation: Measurement principle and static calibration," Review of Scientific Instruments, vol. 82, no. 2, p. 024301, 2011.

[22] S. Kano, Y. Dobashi, and M. Fujii, "Silica nanoparticle-based portable respiration sensor for analysis of respiration rate, pattern, and phase during exercise," IEEE sensors letters, vol. 2, no. 1, pp. 1–4, 2017.

[23] H. Farahani, R. Wagiran, and M. N. Hamidon, "Humidity sensors principle, mechanism, and fabrication technologies: a comprehensive review," Sensors, vol. 14, no. 5, pp. 7881–7939, 2014.

[24] A. K. Kalkan, H. Li, C. J. O'Brien, and S. J. Fonash, "A rapid-response, high-sensitivity nanophase humidity sensor for respiratory monitoring," IEEE electron device letters, vol. 25, no. 8, pp. 526–528, 2004.

[25] A. Gupta, "Respiration Rate Measurement Based on Impedance Pneumography," 2011, Accessed: Feb. 01, 2022. [Online]. Available: https://www.ti.com/lit/an/sbaa181/sbaa181.pdf

[26] C. Massaroni, A. Nicolò, D. Lo Presti, M. Sacchetti, S. Silvestri, and E. Schena, "Contact-based methods for measuring respiratory rate," Sensors, vol. 19, no. 4, p. 908, 2019.

[27] F. Ullah, H. U. Haq, J. Khan, A. A. Safeer, U. Asif, and S. Lee, "Wearable iots and geo-fencing based framework for COVID-19 remote patient health monitoring and quarantine management to control the pandemic," Electronics, vol. 10, no. 16, p. 2035, 2021.

[28] H. R. Touw et al., "Photoplethysmography respiratory rate monitoring in patients receiving procedural sedation and analgesia for upper gastrointestinal endoscopy," Journal of clinical monitoring and computing, vol. 31, no. 4, pp. 747–754, 2017.

[29] I. Alikhani, K. Noponen, A. Hautala, R. Ammann, and T. Seppänen, "Spectral fusion-based breathing frequency estimation; experiment on activities of daily living," BioMedical Engineering OnLine, vol. 17, no. 1, pp. 1–12, 2018.

[30] W. Ma et al., "Optical fiber Fabry–Perot interferometric CO 2 gas sensor using guanidine derivative polymer functionalised layer," IEEE Sensors Journal, vol. 18, no. 5, pp. 1924–1929, 2018.

[31] T.-V. Dinh, I.-Y. Choi, Y.-S. Son, and J.-C. Kim, "A review on non-dispersive infrared gas sensors: Improvement of sensor detection limit and interference correction," Sensors and Actuators B: Chemical, vol. 231, pp. 529–538, 2016.

[32] A. R. A. Sovijarvi, F. Dalmasso, J. Vanderschoot, L. P. Malmberg, G. Righini, and S. A. T. Stoneman, "Definition of terms for applications of respiratory sounds," European Respiratory Review, vol. 10, no. 77, pp. 597–610, 2000.

[33] W. Karlen, A. Garde, D. Myers, C. Scheffer, J. M. Ansermino, and G. A. Dumont, "Estimation of respiratory rate from photoplethysmographic

imaging videos compared to pulse oximetry," IEEE journal of biomedical and health informatics, vol. 19, no. 4, pp. 1331–1338, 2015.
[34] K. Van Loon et al., "Wireless non-invasive continuous respiratory monitoring with FMCW radar: a clinical validation study," Journal of clinical monitoring and computing, vol. 30, no. 6, pp. 797–805, 2016.
[35] M. Ali, H. Shawkey, A. Zekry, and M. Sawan, "One Mbps 1 nJ/b 3.5–4 GHz fully integrated FM-UWB transmitter for WBAN applications," IEEE Transactions on Circuits and Systems I: Regular Papers, vol. 65, no. 6, pp. 2005–2014, 2017.
[36] B.-K. Park, O. Boric-Lubecke, and V. M. Lubecke, "Arctangent demodulation with DC offset compensation in quadrature Doppler radar receiver systems," IEEE transactions on Microwave theory and techniques, vol. 55, no. 5, pp. 1073–1079, 2007.
[37] S.-H. Yu and T.-S. Horng, "Highly linear phase-canceling self-injection-locked ultrasonic radar for non-contact monitoring of respiration and heartbeat," IEEE Transactions on Biomedical Circuits and Systems, vol. 14, no. 1, pp. 75–90, 2019.
[38] O. Kaltiokallio, H. Yiğitler, R. Jäntti, and N. Patwari, "Non-invasive respiration rate monitoring using a single COTS TX-RX pair," in IPSN-14 Proceedings of the 13th International Symposium on Information Processing in Sensor Networks, 2014, pp. 59–69.
[39] C. Chen et al., "TR-BREATH: Time-reversal breathing rate estimation and detection," IEEE Transactions on Biomedical Engineering, vol. 65, no. 3, pp. 489–501, 2017.
[40] S. A. Shah and F. Fioranelli, "RF sensing technologies for assisted daily living in healthcare: A comprehensive review," IEEE Aerospace and Electronic Systems Magazine, vol. 34, no. 11, pp. 26–44, 2019.
[41] X. Mei and H. Ling, "Robust visual tracking and vehicle classification via sparse representation," IEEE transactions on pattern analysis and machine intelligence, vol. 33, no. 11, pp. 2259–2272, 2011.
[42] I. Sato and M. Nakajima, "Non-contact breath motion monitor ing system in full automation," in 2005 IEEE Engineering in Medicine and Biology 27th Annual Conference, 2006, pp. 3448–3451.
[43] T. O. Praktika and A. A. Pramudita, "Implementation of Multi-Frequency Continuous Wave Radar for Respiration Detection Using Software Defined Radio," in *2020 10th Electrical Power, Electronics, Communications, Controls and Informatics Seminar (EECCIS)*, 2020, pp. 284–287.
[44] M. Rehman *et al.*, "Improving machine learning classification accuracy for breathing abnormalities by enhancing dataset," *Sensors*, vol. 21, no. 20, p. 6750, 2021.
[45] [274] A. M. Ashleibta, Q. H. Abbasi, S. A. Shah, M. A. Khalid, N. A. AbuAli, and M. A. Imran, "Non-invasive RF sensing for detecting breathing abnormalities using software defined radios," *IEEE Sens. J.*, vol. 21, no. 4, pp. 5111–5118, 2020.
[46] [275] M. B. Khan, M. Rehman, A. Mustafa, R. A. Shah, and X. Yang, "Intelligent Non-Contact Sensing for Connected Health Using Software Defined Radio Technology," *Electronics*, vol. 10, no. 13, p. 1558, 2021.
[47] [276] M. Rehman *et al.*, "RF sensing based breathing patterns detection leveraging USRP devices," *Sensors*, vol. 21, no. 11, p. 3855, 2021.
[48] Y.-B. Tang and W.-C. Ge, "A novel OFDM symbol synchronisation algorithm based on cyclic prefix in DVB-T," in 2008 4th International Conference on Wireless Communications, Networking and Mobile Computing, 2008, pp. 1–4.
[49] Z. Wang et al., "A survey on CSI-based human behavior recognition in through-the-wall scenario," IEEE Access, vol. 7, pp. 78772–78793, 2019.